HHS Public Access

Author manuscript

Toxicology. Author manuscript; available in PMC 2016 December 02.

Published in final edited form as:

Toxicology. 2015 December 2; 338: 47–58. doi:10.1016/j.tox.2015.10.001.

Subcellular Localization of Rat CYP2E1 Impacts Metabolic Efficiency toward Common Substrates

Jessica H. Hartman[1,‡], **H. Cass Martin**[1,2,‡], **Andres A. Caro**[3], **Amy R. Pearce**[4,5], and **Grover P. Miller**[1,*]

Grover P. Miller: MillerGroverP@uams.edu

[1]Biochemistry and Molecular Biology, University of Arkansas for Medical Sciences, Little Rock, AR

[2]Dept. of Chemistry, University of Central Arkansas, Conway, AR

[3]Dept. of Chemistry, Hendrix College, Conway, AR

[4]Arkansas Biosciences Institute

[5]Psychology & Counseling, Arkansas State University, Jonesboro, AR

Abstract

Cytochrome P450 2E1 (CYP2E1) detoxifies or bioactivates many low molecular-weight compounds. Most knowledge about CYP2E1 activity relies on studies of the enzyme localized to endoplasmic reticulum (erCYP2E1); however, CYP2E1 undergoes transport to mitochondria (mtCYP2E1) and becomes metabolically active. We report the first comparison of in vitro steady-state kinetic profiles for erCYP2E1 and mtCYP2E1 oxidation of probe substrate 4-nitrophenol and pollutants styrene and aniline using subcellular fractions from rat liver. For all substrates, metabolic efficiency changed with substrate concentration for erCYP2E1 reflected in non-hyperbolic kinetic profiles but not for mtCYP2E1. Hyperbolic kinetic profiles for the mitochondrial enzyme were consistent with Michaelis-Menten mechanism in which metabolic efficiency was constant. By contrast, erCYP2E1 metabolism of 4-nitrophenol led to a loss of enzyme efficiency at high substrate concentrations when substrate inhibited the reaction. Similarly, aniline metabolism by erCYP2E1 demonstrated negative cooperativity as metabolic efficiency decreased with increasing substrate concentration. The opposite was observed for erCYP2E1 oxidation of styrene; the sigmoidal kinetic profile indicated increased efficiency at higher substrate concentrations. These mechanisms and CYP2E1 levels in mitochondria and endoplasmic reticulum were used to estimate the impact of CYP2E1 subcellular localization on metabolic flux of pollutants. Those models showed that erCYP2E1 mainly carries out aniline metabolism at all aniline concentrations. Conversely, mtCYP2E1 dominates styrene oxidation at

*Correspondence author at: Department of Biochemistry and Molecular Biology, University of Arkansas for Medical Sciences, 4301 W. Markham, Slot 516. Little Rock, AR 72205, USA; Tel: 501.526.6486; Fax: 501.686.8169.

‡These authors contributed equally to the work.

Declaration of interest: The authors declare they have no conflicts of interest with the contents of this article.

low styrene concentrations and erCYP2E1 at higher concentrations. Taken together, subcellular localization of CYP2E1 results in distinctly different enzyme activities that could impact overall metabolic clearance and/or activation of substrates and thus impact the interpretation and prediction of toxicological outcomes.

Graphical abstract

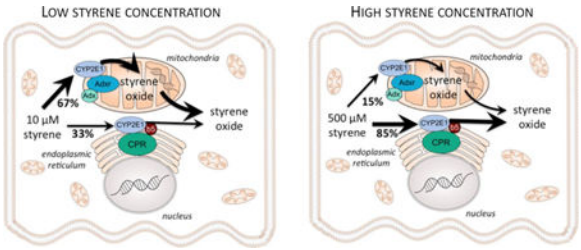

Keywords

CYP2E1; cooperativity; styrene; aniline; 4-nitrophenol; mitochondrial transport

1. Introduction

CYP2E1 plays a central role in the metabolic clearance of small molecules such as endogenous ketone bodies and a wide array of foreign, biologically active (xenobiotic) compounds (Miller 2008). CYP2E1 reactions often eliminate potentially toxic compounds and paradoxically, bioactivate others into toxicants or carcinogens. Moreover, oxidative reactions carried out by CYP2E1 can lead to formation of reactive oxygen species and then oxidative stress due to poorly coupled oxygen activation by CYP2E1 and redox partners. These metabolic processes alone and in combination contribute to toxicological responses associated with CYP2E1 activity toward drugs (acetaminophen), pollutants (aniline and styrene) and other compounds (ethanol). An understanding of the correlation between metabolism and toxicity requires knowledge of CYP2E1 metabolic efficiency toward substrates. An important strategy to obtain this information relies on in vitro steady-state metabolic studies with subcellular fractions that tease out the details of CYP2E1 mechanisms and constants.

CYP2E1 localizes to the endoplasmic reticulum (erCYP2E1) and requires cytochrome P450 reductase as an obligate redox partner for activity. This functional form of CYP2E1 was first identified from hepatic microsomal fractions by its high selectivity toward hydroxylation of 4-nitrophenol (Koop 1986). Kinetic profiles for erCYP2E1 substrates are often hyperbolic and thus best fit to the Michaelis-Menten equation in which the metabolic efficiency is constant. A more complex array of mechanistic possibilities is appropriate in light of recent steady-state studies, such as those for aniline (Hartman et al. 2014a), styrene (Hartman et al. 2012), and *m*-xylene (Harrelson et al. 2008). The metabolism of those erCYP2E1 substrates involved non-hyperbolic kinetic profiles, whereby metabolic efficiency either increased (positive cooperativity) or decreased (negative cooperativity or substrate inhibition) as a function of substrate concentration. Those shifts in metabolic efficiencies indicated changes

in contributions from more than one form of CYP2E1 to the reaction that may derive from mechanisms involving catalytic and effector sites for erCYP2E1 (Collom et al. 2008; Hartman et al. 2012, 2013a; Hartman et al. 2013b; Hartman et al. 2014a; Hartman et al. 2014b; Levy et al. 2015; Pianalto et al. 2013). Their presence and specificities were further characterized through experimental catalytic inhibition (Collom et al. 2008; Hargreaves et al. 1994; Hartman et al. 2013b) and binding (Collom et al. 2008; Hartman et al. 2013b) studies and computational docking and Molecular Dynamics simulations (Levy et al. 2015) using a series of mono- and bi-cyclic azoles. Failure to account for the two-site mechanism may compromise the interpretation and prediction of the role of CYP2E1 in the metabolic clearance or activation of substrates.

In vivo clearance models based on in vitro kinetics revealed significant differences between the traditional Michaelis-Menten mechanism and cooperative metabolic processes observed for aniline (Hartman et al. 2014a) and especially styrene (Hartman et al. 2012). In fact, in vivo gas-uptake data revealed a bi-phasic process for dichloromethane metabolism that could be explained through a physiologically based pharmacokinetic model incorporating a two-binding site CYP2E1 mechanism (Evans and Caldwell 2010). These findings underscore the need to further explore the prevalence and significance of the two-binding site mechanism in CYP2E1 metabolism.

Much of our understanding of CYP2E1 activity and its importance rely on studies focused on its form localized to the endoplasmic reticulum; however, CYP2E1 undergoes transport to the mitochondria (Neve and Ingelman-Sundberg 1999; Robin et al. 2002) in a regulated process (Anandatheerthavarada et al. 1997; Robin et al. 2002; Sangar et al. 2010) and becomes functional upon association with adrenodoxin and adrenodoxin reductase (Robin et al. 2001). The functional properties and significance of mtCYP2E1 are only now being explored through in vitro cell-based and subcellular fraction studies. There is high inter-individual variability in the amount of CYP2E1 localized in the hepatic mitochondrial and microsomal fractions, which can be partially explained by genetics (Bansal et al. 2013). Specifically targeting CYP2E1 for sole expression in the mitochondria of HepG2 or COS-7 cells leads to higher levels of reactive oxygen species and oxidative stress, mitochondrial dysfunction and cytotoxicity (Bai and Cederbaum 2006; Knockaert et al. 2011). In fact, these outcomes are driven more by mtCYP2E1 than erCYP2E1 in cells exposed to the CYP2E1 substrates acetaminophen and ethanol (Knockaert et al. 2011). Subcellular fractionation studies revealed that mtCYP2E1 metabolizes typical erCYP2E1 substrates including 4-nitrophenol, dimethylnitrosamine, and chlorzoxazone (Bai and Cederbaum 2006; Robin et al. 2001). Nevertheless, none of those studies measured the metabolic efficiency of the mtCYP2E1 reactions or the levels of CYP2E1 between the mitochondrial or endoplasmic reticulum compartments. This lack of detailed kinetic studies with subcellular fractions precludes comparing and assessing quantitatively the relative roles and consequences of mtCYP2E1 and erCYP2E1 in substrate metabolism.

In this study, we determined metabolic mechanisms and constants for erCYP2E1 and mtCYP2E1 toward substrates as a basis for modeling clearance through subcellular compartments. We isolated mitochondrial and microsomal liver fractions pooled from six untreated adult female Sprague-Dawley rats and measured CYP2E1 levels present in

subcellular fractions by Western blot using recombinant CYP2E1 as a standard. For steady-state studies, we chose three substrates to assess whether mtCYP2E1 is capable of the same diversity of metabolic mechanisms as erCYP2E1, namely, substrate inhibition (4-nitrophenol) (Collom et al. 2008; Koop 1986), negative cooperativity (aniline) (Hartman et al. 2014a), and positive cooperativity (styrene) (Hartman et al. 2012). Initially, we verified the role of CYP2E1 from both subcellular compartments on targeted reactions through inhibitor phenotyping experiments. Next, published steady-state protocols (Collom et al. 2008; Hartman et al. 2012; Hartman et al. 2014a) were carried out to obtain kinetic profiles for all three reactions. The resulting data were normalized to the amount of CYP2E1 present in the reaction and compiled for global fitting to six possible mechanisms involving a single binding site (Michaelis-Menten) or two binding sites. The most statistically probable one among them was identified using DynaFit software (Kuzmic 1996) as described (Collom et al. 2008; Hartman et al. 2012; Hartman et al. 2014a). Lastly, we compared the metabolic efficiencies between mtCYP2E1 and erCYP2E1 for substrates and then modeled their collective contribution to substrate clearance through their respective subcellular compartments.

2. Experimental Procedures

2.1 Chemicals

All chemicals were ACS grade or higher and purchased from Sigma Aldrich, St Louis, MO: 4-nitrophenol, 4-nitrocatechol, 4-aminophenol, 2,6-dichloroindophenol, phenol, sodium carbonate, trichloroacetic acid, 4-methylpyrazole, and metyrapone. The protease/phosphatase inhibitor cocktail was prepared in-house using the Roche cOmplete® mini EDTA-free tablets from Life Sciences and a phosphatase inhibitor cocktail containing sodium fluoride, sodium pyrophosphate, and sodium orthovanadate. Distilled aniline was kept under argon until needed for experimentation. HPLC grade methanol and acetonitrile were purchased from Fisher Scientific, Wilmington, MA. Liver tissue from adult female Sprague Dawley rats was supplied by Arkansas Biosciences Institute, Jonesboro, AR.

2.2 Subcellular Fractionation

Mitochondrial and microsomal rat liver samples were isolated and purified using subcellular fractionation techniques. In a typical preparation, 0.75 g tissue was homogenized in 1.5 mL Homogenization Buffer (10 mM potassium phosphate, pH 7.4, 10 mM EDTA, 1.15% KCl, and protease/phosphatase inhibitor cocktail) using ten smooth, twisting strokes with 2 mL homogenization glassware. Homogenate was centrifuged at 4°C, 2500 × *g* for 10 min. Supernatant was centrifuged a second time at 4°C, 9000 × *g* for 20 min. Pellet was stored for mitochondrial isolation in further fractionation steps. Supernatant was centrifuged at 4°C, 100,000 × *g*.

2.3 Purification of Microsomal Fraction

The pellet from the subcellular fractionation was resuspended in homogenization buffer with a 1 mL tissue grinder using seven smooth, twisting strokes. The resulting homogenate was centrifuged at 4°C, 100,000 × *g* for 60 min. The supernatant was discarded and the pellet resuspended in 0.25 mL 250 mM sucrose with a 1 mL tissue grinder using seven smooth,

twisting strokes. Homogenates containing isolated and purified microsomal fractions were stored at -80°C until needed for kinetic assays.

2.4 Isolation of Mitochondrial Fraction

The crude mitochondrial pellet from initial fractionation steps was resuspended in 3 mL SEM Buffer (250 mM sucrose, 1 mM EDTA, 10 mM MOPS/KOH, pH 7.2). Suspension was added to a sucrose gradient consisting of 1.5 mL 60% (w/v) sucrose in EM Buffer (1 mM EDTA, 10 mM MOPS/KOH, pH 7.2), 4 mL 32% (w/v) sucrose in EM Buffer, 1.5 mL 23% (w/v) sucrose in EM Buffer, and 1.5 mL 15% (w/v) sucrose in EM Buffer layered respectively in a Beckman SW28 centrifuge tube. Gradient was centrifuged in a Beckman SW28.1 swinging bucket rotor at 4°C, 28,000 rpm (140,000 × *g*) for 60 min. Mitochondrial pellet was a band superficial to the 60% sucrose layer and was removed and subsequently resuspended in 12 mL SEM Buffer. The resulting suspension was centrifuged at 4°C, 23,000 rpm (95,000 × *g*) for 30 min in the SW28.1 swinging bucket rotor. The pellet was resuspended in 200 μL SEM Buffer and sonicated to homogeneity using a Branson Sonifier® 250 (Emerson Industrial, Danbury, CT) with a tapered probe (20% duty, two 10-second bursts followed by 30-second cooling). Isolated and purified mitochondrial fraction was stored at -80°C until needed for kinetic assays.

2.5 Western blot analysis for determination of fraction purity and CYP2E1 concentration

Protein content from mitochondrial and microsomal fractions was determined using the BCA assay.(Smith et al. 1985) Total P450 from mitochondrial and microsomal fractions was determined using the reduced CO spectra, as described (Guengerich et al. 2009). Human CYP2E1 Supersomes® (Corning Gentest, Corning, NY) were used as an authentic standard for quantification of CYP2E1 in subcellular fractions. Varying amounts of samples and standards were loaded and resolved by SDS-polyacrylamide electrophoresis (10% gels, w/v). After transferring separated proteins to nitrocellulose membranes, they were immunoblotted with specific antibodies against SDHA (Abcam; ab14711), SERCA (Santa Cruz; sc30110), and CYP2E1 (Abcam; ab19140). The membranes were then incubated with the corresponding secondary horseradish-conjugated antibody and immunoreactive bands were visualized by chemiluminescence (Chemiglow; Protein Simple, Santa Clara, CA) using a FluorChem FC3 System (ProteinSimple, San Jose, CA, USA). Membranes were stripped and re-probed with colloidal gold solution (Biorad Laboratories, Hercules, CA) for nonspecific proteins as a loading control. The density of protein bands was quantitatively analyzed by ImageJ software (NIH; Bethesda, MD) and expressed as a relative ratio against the loading control. Both standards and samples were quantified within the linear range of the response (Charette et al. 2010). The concentration of CYP2E1 was then determined based on a calibration curve from the human CYP2E1 standards and used to normalize kinetic rates of metabolism for comparison of the intrinsic CYP2E1 activity between fractions.

2.6 4-Nitrophenol Kinetic Assay

We examined steady-state metabolism of 4-nitrophenol by hydroxylation of the 3- position to yield 4-nitrocatechol. For each reaction using microsomal fractions, 0.5 mg/mL protein

was incubated with eight different 4-nitrophenol concentrations ranging from 31 to 2000 μM in 50 mM potassium phosphate pH 7.4 at 37°C. Reactions were initiated with 1 mM NADPH, and after 30 minutes of incubation, the reactions were quenched with an equal volume of a solution containing 0.4 N perchloric acid and 25 μM 4-nitroanisole (internal standard). The quenched reaction was centrifuged to remove precipitated proteins and the resulting supernatant analyzed by HPLC with absorbance detection at 360nm to quantitate product. Final 4-nitrocatechol concentrations were determined using calibration curves with authentic standards. Under these conditions, product formation was linear with respect to time and protein concentration (data not shown). Similar experiments were carried out for mitochondrial reactions at 2 mg/mL mitochondrial protein.

2.7 Aniline Kinetic Assay

We examined steady-state metabolism of aniline to 4-aminophenol according to previously described methods (Hartman et al. 2014a). For each reaction using microsomal fractions, 0.5 mg/mL protein was incubated with eight different aniline concentrations ranging from 2.5 to 500 μM in 50 mM potassium phosphate, pH 7.4 at 37°C. Reactions were initiated with 1 mM NADPH, and after 30 min, the reactions were quenched with an equal volume of a solution containing 0.4 N trichloroacetic acid solution. The quenched reaction was centrifuged and the resulting supernatant was added to phenol in the presence of Na_2CO_3 to conjugate unstable 4-aminophenol (product) to phenol for ultimately creating indophenol. Final indophenol concentrations were determined using HPLC with absorbance detection at 630nm. Calibration curves were generated with freshly prepared authentic 4-aminophenol standards relative to 2,6-dichloroindophenol (internal standard). Under these conditions, product formation was linear with respect to time and protein concentration (data not shown). Comparable assays were carried out with mitochondrial samples at 2 mg/mL protein.

2.8 Styrene Kinetic Assay

We examined steady-state metabolism of styrene to styrene oxide according to previously described methods (Hartman et al. 2012). For each reaction using microsomal fractions, 0.5 mg/mL protein was incubated with eight different styrene concentrations ranging from 5 to 500 μM in 50 mM potassium phosphate, pH 7.4 at 37°C. Reactions were initiated with 1 mM NADPH, and after 30 minutes, the reactions were quenched with an equal volume (25 μL) of a solution containing saturated barium hydroxide and 25 μL of a 10% solution of zinc sulfate containing 10 μM benzyl alcohol (internal standard). Under these conditions, all styrene oxide was converted to styrene glycol. The quenched reaction was centrifuged and the resulting supernatant was analyzed by HPLC with UV detection at 200nm to quantitate product. Final product concentrations were determined using calibration curves with authentic standards. Under these conditions, product formation was linear with respect to time and protein concentration (data not shown). Comparable assays were carried out with mitochondrial samples at 2 mg/mL protein.

2.9 Statistical analysis of steady-state kinetic mechanisms

Using the kinetic data, we investigated the mechanism and parameters for equilibrium constants and reaction rates using DynaFit version 3.28 (Biokin, Ltd., Watertown, MA) as

described previously (Hartman et al. 2012, 2013a; Hartman et al. 2013b; Hartman et al. 2014a; Pianalto et al. 2013). Briefly, the analysis involved globally comparing fits of kinetic data to six steady-state mechanisms involving one binding site for substrate (Michaelis-Menten) or two binding sites for substrate. Two-site mechanisms involve formation of a binary (ES) complex and a ternary (ESS) complex, both of which can be catalytically active. In this analysis, binding events are ordered with respect to stoichiometry (number of bound molecules) but not in respect to occupancy of each binding site.

2.10 Inhibitor phenotyping of P450 activity present in rat liver microsomes and mitochondria

For inhibitor phenotyping experiments, 0.5 mg/mL rat liver microsomes or 2 mg/mL rat liver mitochondria were incubated with 50 or 500 μM substrate (4-nitrophenol, aniline, or styrene), 1 mM NADPH, and a specific P450 chemical inhibitor in 50 mM potassium phosphate buffer, pH 7.4. The inhibitors used in these experiments were chrysin (1 μM) for CYP1A, tranylcypromine (2 μM) for CYP2A, metyrapone (25 μM) for CYP2B, sulfaphenazole (10 μM) for CYP2C, 4-methylpyrazole (4MP; 40 μM) for CYP2E1, and ketaconazole (1 μM) for CYP3A. The inhibitors included in each experiment were chosen based on reported contribution of that isoform to metabolism of the substrate in humans or rodents.(Hartman et al. 2012, 2013a; Hartman et al. 2014a; Pianalto et al. 2013) After addition of NADPH, samples were incubated at 37°C for 30 min and analyzed as described for steady-state experiments. Due to low solubility, all inhibitor stocks were prepared in methanol, and added to reactions yielding a final 0.5% methanol (v/v) to minimize the impact on rat CYP2E1 activity (Li et al. 2010). The statistical significance of the effect of inhibitors on metabolism was determined using a one-way analysis of variance (ANOVA) test performed in GraphPad Prism 5.0 (San Diego, CA).

3. Results

3.1 Metabolic capacity of CYP2E1 based on subcellular levels

Detailed kinetic studies for CYP2E1 required fractionation of the liver homogenate into mitochondrial and microsomal fractions using standard protocols for the isolation and purification of each (Cohen et al. 2008; Gregg et al. 2009; Velick and Strittmatter 1956). The purity of each fraction was verified by immunoblotting using succinate dehydrogenase (SDHA) as a marker for mitochondria and the sarco-endoplasmic reticulum Ca^{2+}-ATPase (SERCA) as a marker for microsomes. Cross-contamination between the microsomal and mitochondrial fractions was low, as shown by the ratio of the band intensity of the mitochondrial marker SDHA in the mitochondrial fraction compared with SDHA in the microsomal fraction (average 3.2), and the ratio of the band intensity of the microsomal marker SERCA in the microsomal fraction compared with SERCA in the mitochondrial fraction (average 3.9) (Figure 1, Panel A).

After verifying fraction purity, the total amount of CYP2E1 in each fraction was measured by immunoblot (Figure 1, Panel B) and quantified using densitometry compared to authentic commercially obtained CYP2E1 standards (Corning Gentest Human CYP2E1 Supersomes®). In our study, the total protein in each final purified fraction differed by

approximately two-fold (Figure 1, Panel C), and the total P450 per mg protein was approximately four-fold greater in the microsomal versus mitochondrial fractions (Figure 1, panel D**)**. Interestingly, under these conditions, the total CYP2E1 per mg protein was similar between the two fractions (Figure 1, panel E). In terms of total yield, there were similar total protein yields in each purified fraction (data not shown).

3.2 4-Nitrophenol: Subcellular localization impacts CYP2E1 metabolic efficiency but not selectivity

Inhibitor phenotyping studies revealed the major role of CYP2E1 in 4-ntirophenol metabolism. Recombinant human CYP2E1 and CYP3A4 metabolize 4-nitrophenol (Zerilli et al. 1997), yet CYP3A4 is only found in the microsomal fraction unlike CYP2E1.(Robin et al. 2002) The presence of 4-methylpyrazole, a CYP2E1-specific inhibitor (Halpert et al. 1994; Newton et al. 1995), suppressed metabolism of 4-nitrophenol by 70-80% for both fractions regardless of substrate concentration, while ketoconazole, an inhibitor of CYP3A4 activity (Newton et al. 1995), had no effect (Figure 2). Taken together, erCYP2E1 and mtCYP2E1 were primarily responsible for hydroxylating 4-nitrophenol to 3,4-nitrocatechol indicating this reaction remains an attractive CYP2E1-specific marker reaction.

Steady-state studies showed that subcellular localization of CYP2E1 significantly impacted the efficiency of 4-nitrophenol metabolism (Figure 3, Panel A; Table 1). The non-hyperbolic kinetic profile for erCYP2E1 reflected substrate inhibition in which a rapid rise in the initial rate was followed by decreases at higher substrate concentrations. Among six possibilities, the most probable mechanism explaining the observed kinetic profile involved two binding sites. In that mechanism, the substrate had higher affinity for the first binding event ($K_S \ll K_{SS}$) and only the binary complex was catalytically active.

By contrast, the hyperbolic kinetic profile for mtCYP2E1 oxidation of 4-nitrophenol was best explained by the traditional Michaelis-Menten mechanism (Figure 3, Panel B; Table 1). In this case, substrate bound to a single binding site on the enzyme for catalysis to occur. Despite different mechanisms, the K_m value of 4-nitrophenol for the mtCYP2E1 site was similar to that observed for erCYP2E1. The resulting Michaelis enzyme-substrate complexes were not equivalent as evidenced by a nine-fold lower turnover rate observed for mtCYP2E1.

3.3 Aniline: Decrease in CYP2E1 metabolic efficiency depends on subcellular localization

Multiple P450s are capable of hydroxylating aniline, and thus we carried out inhibitor phenotyping to establish the significance of CYP2E1 in the reaction (Figure 4). Compounds targeting CYP1A and CYP2C did not affect aniline hydroxylation by either subcellular fraction and thus their contributions were negligible. On the other hand, inhibitors for CYP2A and CYP2E1 significantly blocked activity present in microsomal and mitochondrial reactions at low and high aniline concentrations.

The metabolism of aniline by rat liver microsomes resulted in a significantly bi-phasic, non-hyperbolic profile that reflected negative cooperativity (Figure 5, Panel A; Table 1). Based on Akaike Information Criterion, the most favored mechanism explaining these data was a

two-site cooperative mechanism in which catalytically active enzyme-substrate complexes formed with one or two substrate molecules bound to the enzyme. In this mechanism, the first aniline molecule bound to erCYP2E1 with the highest affinity among all substrates in this study and formed a catalytically component complex. At higher aniline concentrations, a second molecule bound to the enzyme-substrate complex weakly (25-fold less than the first binding event). Nevertheless, the resulting ternary complex displayed a two-fold higher rate of turnover than the initial binary enzyme-substrate complex. In combination, these mechanistic steps decreased metabolic efficiency as a function of aniline concentration due to a more significant drop in substrate binding relative to the rise in rate of turnover.

Mitochondrial CYP2E1 activity toward aniline led to a hyperbolic kinetic profile that best fit statistically to a simple one-site (Michaelis-Menten) mechanism (Figure 5, Panel B; Table 1). Based on the K_m, substrate affinity for mtCYP2E1 was intermediate between the two binding sites observed for erCYP2E1. The resulting Michaelis enzyme-substrate complex for the mitochondrial enzyme was much less effective at turnover, however. The corresponding rate was 10- and 20-fold lower than that observed for the microsomal enzyme following the first and second substrate binding events respectively. Similar to the observations for 4-nitrophenol metabolism, subcellular localization seems to alter binding interactions with aniline in terms of affinity and stoichiometry as well as the subsequent hydroxylation of the substrate.

3.4 Styrene: Increase in CYP2E1 metabolic efficiency depends on subcellular localization

Inhibitor phenotyping experiments with styrene revealed that only CYP2E1-specific 4-methylpyrazole significantly decreased styrene metabolism present in both subcellular fractions (Figure 6). Inhibitors targeting CYP1A, CYP2B1/2, and CYP2C had no effect on the reaction despite studies implicating their role in styrene metabolism (Kim et al. 1997; Nakajima et al. 1994). Regardless of subcellular localization, CYP2E1 is primarily responsible for styrene epoxidation into a genotoxic metabolite.

Styrene metabolism by rat liver microsomes exhibited a sigmoidal kinetic profile (Figure 7, Panel A; Table 1). In a comparative analysis of six mechanisms, the statistically preferred one was a two-site cooperative mechanism for erCYP2E1. The first molecule of styrene bound to the enzyme relatively weakly to form a catalytically non-productive enzyme-substrate complex. A second molecule then bound with three-fold greater affinity to the enzyme-substrate complex to form the catalytically competent ternary complex leading to product formation. The combination of these events led to a sigmoidal kinetic profile as the metabolic efficiency increased with styrene concentration.

Transport of CYP2E1 to mitochondria led to an enzyme whose metabolic efficiency remained constant as shown by a hyperbolic kinetic profile (Figure 7, Panel B; Table 1). Statistically, the data fit best to a one-site model (Michaelis-Menten kinetics) involving a single binding site for substrate. Interestingly, substrate affinity for mtCYP2E1 was similar to that observed for the second binding event to erCYP2E1. While the Michaelis-Menten complex formed readily for mtCYP2E1, the rate of turnover was six-fold slower than that observed for erCYP2E1. Differences between the rates were not as significant as those for

hydroxylation of 4-nitrophenol and aniline, suggesting that mtCYP2E1 may more readily generate toxic epoxides than hydroxylated metabolites.

3.5 Modeling CYP2E1 substrate clearance through subcellular compartments

We estimated the impact of CYP2E1 subcellular localization on the metabolic flux of pollutants through mitochondria and endoplasmic reticulum based on mechanisms and constants determined in this study. For aniline and styrene, the rate was estimated based on the fit to each model for a low (10 μM) and high (500 μM) concentration, assuming equal protein levels for CYP2E1 in each compartment. The total rate was considered to be the sum of the rates for each compartment and the relative contribution of each compartment was expressed as the percent of the total rate of metabolism at that concentration.

Models for substrate clearance through subcellular compartments indicated minimal effects for the pollutant aniline. At low concentrations, approximately 94% of aniline metabolism occurred through erCYP2E1 and only about 6% of total aniline hydroxylation was carried out by mtCYP2E1. At higher concentrations, the distribution was very similar with 95% of metabolism occurring at the endoplasmic reticulum. Therefore, at least for aniline, it seems that CYP2E1 metabolism is more significant in the endoplasmic reticulum compared to that in mitochondria.

On the other hand, the model yielded very striking results for the metabolic flux of styrene through these subcellular compartments. At low concentrations (10 μM), two-thirds of styrene metabolism occurred in mitochondria, while only one-third went through the endoplasmic reticulum (Figure 8, Panel A). Although unlikely under in vivo conditions, higher styrene concentrations (500 μM) displayed a shift to primarily (85%) metabolism in the endoplasmic reticulum due to increased metabolic efficiency observed for erCYP2E1 (Figure 8, Panel B).

4. Discussion

Herein, we show that CYP2E1 localization to mitochondria and endoplasmic reticulum (er) determined metabolic mechanisms toward the marker substrate 4-nitrophenol and two common pollutants, i.e. aniline and styrene. Inhibitor phenotyping experiments confirmed that the observed activity toward all three substrates reflected mainly CYP2E1 contributions regardless of subcellular localization. The kinetic experiments showed that the metabolic efficiency of mtCYP2E1 toward all three substrates was constant as reflected in a hyperbolic (Michaelis-Menten) kinetic profile, while those for erCYP2E1 changed with substrate concentration in ways that depended on the specific substrate. As reported previously with microsomal studies (Collom et al. 2008; Hartman et al. 2012, 2013a; Hartman et al. 2014a; Pianalto et al. 2013), non-hyperbolic kinetic profiles for erCYP2E1 revealed changes in metabolic efficiencies during the reaction consistent with substrate inhibition (4-nitrophenol), negative cooperativity (aniline), and positive cooperativity (styrene). Based on these CYP2E1 mechanisms, clearance models indicated that the relative significance of CYP2E1 localization on the metabolic flux of pollutants through the cell was substrate dependent and thus requires further study.

Compared to previous efforts (Addya et al. 1997; Bai and Cederbaum 2006; Knockaert et al. 2011; Neve and Ingelman-Sundberg 1999; Robin et al. 2002; Robin et al. 2001; Sangar et al. 2010), the design of these studies yielded a more quantitative assessment of the impact of subcellular localization on CYP2E1 activity and role in metabolic clearance and/or activation of substrates. We determined the amount of total protein, P450, and CYP2E1 for scaling relative abundances and then normalized enzyme activity to CYP2E1 levels in contrast to the work of others. Typically, the apparent activity is normalized to total protein, yet this approach reflects variations in all proteins and not CYP2E1 itself and hence precludes an accurate comparison of CYP2E1 activities between subcellular fractions. Like others, a potential limitation of our work was the isolation of obligate redox partners for mtCYP2E1 due to their peripheral association with the membrane. Their loss during fractionation would decrease the observed CYP2E1 activity from mitochondrial preparations such that the reported values are a possible minimum value for mtCYP2E1 contributions to metabolism relative to erCYP2E1. This possibility does not apply to erCYP2E1, because cytochrome P450 reductase present at the endoplasmic reticulum is an integral membrane protein.

Overall, this approach provided an ideal system for comparison of CYP2E1 activity between mitochondria and microsomes (er) from rat liver and would likely extrapolate to CYP2E1 present in humans and other species. CYP2E1 is evolutionarily conserved among vertebrates and shares a high sequence identity between humans, rats, and mice (Martignoni 2006) related to the current studies. The various forms of CYP2E1 demonstrate similar substrate selectivity and efficiency between mouse, rat, and human (although the expression level varies between species). These properties even apply to non-Michaelis-Menten mechanisms in which metabolic efficiency changes during the reaction according to data on 4-nitrophenol metabolism of by rabbit (Collom et al. 2008), rat (F344) (Pianalto et al. 2013), mouse (B6C3F1) (Pianalto et al. 2013), and human erCYP2E1 (Hartman et al. 2013a), aniline hydroxylation by human erCYP2E1 (Hartman et al. 2014a), and styrene epoxidation by human erCYP2E1 (Hartman et al. 2012). Therefore, the results from these kinetic experiments with rat enzymes would likely apply to human CYP2E1 activity and reflect potential impacts on associated toxicity from metabolism occurring in each compartment.

Steady-state kinetic experiments focused on three substrates to assess whether mtCYP2E1 was capable of the same diversity of metabolic mechanisms as erCYP2E1. Metabolic clearance of the model substrate 4-nitrophenol is not toxicologically relevant; nevertheless, the high selectivity and efficiency of CYP2E1 metabolism of 4-nitrophenol make the reaction an ideal surrogate for tracking CYP2E1 activity in a wide range of in vitro and in vivo studies (Amato et al. 1998; Tassaneeyakul et al. 1993). This premise was supported by our inhibitor phenotyping studies, which implicated a role for CYP2E1 and no contribution of rat CYP3A. In steady-state kinetic experiments with erCYP2E1, metabolic efficiency decreased with increasing levels of 4-nitrophenol that resulted in substrate inhibition. This transition was absent for mtCYP2E1, and the kinetic profile conformed to Michaelis-Menten kinetics. Based on K_m values the affinity of 4-nitrophenol for the mtCYP2E1 site was similar to that observed for erCYP2E1, suggesting subcellular localization did not alter binding contacts for this common marker substrate.

Aniline is a common industrial chemical (Sittig 1981) found in industrial waste and a constituent of Superfund sites (ATSDR 2011). CYP2E1 dominated aniline hydroxylation in both organelles with minor CYP2A contributions in microsomes according to phenotyping experiments. While those experiments suggested minor CYP2A contributions to mitochondrial metabolism, those results were likely an artifact due to possibly cross-interaction with CYP2E1 (Taavitsainen et al. 2001; Zhang et al. 2001) and absence of CYP2A in mitochondria. The subcellular localization of CYP2E1 altered aniline binding affinity and stoichiometry as well as subsequent hydroxylation. Steady-state mtCYP2E1 oxidation of aniline displayed simple Michaelis-Menten kinetics, while similar to 4-nitrophenol, erCYP2E1 metabolism involved a two-site negative cooperative mechanism with an overall decrease in enzyme efficiency. Nevertheless, when compared to the mitochondrial enzyme, erCYP2E1 was consistently more effective at metabolizing aniline due to higher initial substrate affinity and rate of turnover even after the association of a second, low affinity aniline molecule.

Styrene is present in cigarette smoke, diesel exhaust, and some industrial waste, and therefore may represent a potential health threat as a class 2B carcinogen (2008; Barale 1991; Bond and Bolt 1989). Bioactivation of styrene involves epoxidation of the double bond through a reaction catalyzed mainly by CYP2E1 (Kim et al. 1997; Mendrala 1993; Nakajima et al. 1994), and our studies confirmed this role for CYP2E1 localized to both rat liver microsomal and mitochondrial fractions. The affinity of styrene for erCYP2E1 was poor initially and then increased to yield a catalytically active CYP2E1 as reflected in a positively cooperative kinetic profile. As observed for aniline and 4-nitrophenol, mtCYP2E1 metabolism involved a simple Michaelis-Menten mechanism with no change in metabolic efficiency across the range of styrene concentrations. The affinity for substrate was comparable to that observed for the second binding event with erCYP2E1 that yielded the catalytically active form of the enzyme. Taken together, erCYP2E1 required an initial styrene molecule to bind for catalysis to occur, whereas mtCYP2E1 did not, suggesting possible structural difference between these CYP2E1 isoforms.

Differences between mtCYP2E1 and erCYP2E1 may arise from characteristic substrate interactions, redox partner preferences, and structural elements. First, we revealed that the metabolic efficiency for mtCYP2E1 toward 4-nitrophenol, aniline, and styrene remained constant, whereas those values either decreased or increased as a function of substrate concentration during erCYP2E1 metabolism. Those outcomes reflected differences in substrate structure indicating erCYP2E1 and mtCYP2E1 possess distinct substrate specificities and catalytic capacities. Second, CYP2E1 metabolic properties depend on redox partners, namely adrenodoxin/adrenodoxin reductase (mtCYP2E1) or cytochrome P450 reductase and possibly cytochrome b_5 (erCYP2E1) (Robin et al. 2001). These protein-protein interactions may impact CYP2E1 conformations like an allosteric effector and/or alter electron transfer steps involved in oxygen activation. The rate-limiting step during P450 catalysis typically involves electron transfer steps during oxygen activation(Guengerich 2002) and thus it seems likely that redox partners for CYP2E1 contribute to metabolic efficiency toward substrates. Third, subcellular localization of CYP2E1 influences enzyme conformations. CYP2E1 purified from microsomal and mitochondrial fractions possess different secondary structural elements based on circular

dichroism spectra (Robin et al. 2001). Unique conformations of erCYP2E1 and mtCYP2E1 could explain the presence or absence of a second substrate-binding site. Moreover, the overall fold must differ between them, because they only associate with redox partners derived from the original subcellular compartment. erCYP2E1 will reconstitute a catalytically active complex only with cytochrome P450 reductase and mtCYP2E1 with adrenodoxin/adrenodoxin reductase (Robin et al. 2001). Taken together, the subcellular localization of CYP2E1 yields functionally and structurally distinct enzymes that would likely impact the role of CYP2E1 in toxicological processes.

We modeled the impact of CYP2E1 subcellular localization on the predicted metabolic flux of pollutants through mitochondria and endoplasmic reticulum based on mechanisms and constants determined in this study assuming equal protein levels of CYP2E1 in each compartment. Previous studies have demonstrated high inter-individual variability in CYP2E1 levels in mitochondria and microsomes (Bansal et al. 2013), which could result in a shift in this flux. Models for substrate clearance through subcellular compartments indicated minimal effects for the pollutant aniline, with the majority of aniline clearance occurring in the ER. On the other hand, the model yielded very striking results for the metabolic flux of styrene through these subcellular compartments, as depicted in Figure 8. At low styrene concentrations, metabolism by mtCYP2E1 was most important. The common emphasis on erCYP2E1 metabolism would then underestimate styrene activation to the epoxide metabolite under these conditions. In fact, individuals, such as workers in the polymer industry, were previously exposed to higher levels of styrene and report plasma levels of styrene up to 22 μM (Löf 1986; Prieto 2002; Somorovska 1999); however, more recent studies of industrial workers suggest exposures are lower and result in styrene plasma levels reaching only 0.06 μM (Bonanni et al. 2015). The difference between assumed and actual metabolic activation of styrene would be even larger for more common environmental exposures of less than 10 μM. erCYP2E1 metabolism of styrene only became dominant at higher styrene concentrations that are not physiologically probable. Overall, this dynamic shift in the relative contributions of CYP2E1 in different subcellular compartments was more significant for styrene than aniline due to the respective changes in metabolic efficiencies; none of those effects on metabolism and the consequences of those processes would occur if CYP2E1 metabolism of substrates always conformed to Michaelis-Menten kinetics as currently assumed.

Importantly, these estimations reflected contributions solely from CYP2E1 activity and not other processes like transport and conjugation. The efficiencies of those processes could differ between compartments and impact the toxicological consequences of CYP2E1 activity and thus they should be explored further. Additionally, the probability of cellular toxicity associated with CYP2E1 bioactivation of compounds may depend on the subcellular compartment in which those bioactive compounds are produced. Finally, there may be interspecies differences in these processes between rodents and humans and thus care should be taken in extrapolating the potential impacts of these findings directly to humans. However, these efforts are the first crucial step toward characterizing the production of bioactive compounds in each compartment and determining the relative importance of CYP2E1 metabolism in each subcellular location.

These clearance models for CYP2E1 provide an important baseline highlighting the effects of metabolic efficiencies on substrate metabolism in different subcellular organelles, yet alterations in the regulation of CYP2E1 expression and transport to those compartments will similarly play a role in their relative significance in metabolism. Induction and accumulation of mtCYP2E1 has been observed in streptozotocin-induced diabetic rats (Raza et al. 2004), in rats treated with the CYP2E1 inducer pyrazole (Robin et al. 2001), and in mice and cultured rat hepatocytes exposed to ethanol (Robin et al. 2005). Importantly, ethanol induction of mtCYP2E1 resulted in depleted cellular glutathione, contributing to increased oxidative stress. Variation in distribution of CYP2E1 between the mitochondria and microsomes has also been reported for a bank of human livers (Bansal et al. 2013), and the authors attributed some of this variability to genetic polymorphisms in the N-terminal targeting sequence of CYP2E1 and the remaining cause for this variation require further study. An additional layer of complexity is our substrate-dependent change in metabolic efficiency significantly that impacts the contributions from these subcellular compartments on clearance and ultimately bioactivation to toxic metabolites.

Concluding Remarks

We present strong evidence illustrating the impact of CYP2E1 subcellular localization on metabolic efficiency toward well-known substrates. Much of what is understood about the toxicological significance of CYP2E1 derives solely from studies on erCYP2E1 present in microsomal fractions and thus may not be accurate. Beyond current work presented here and in previous studies (Bai and Cederbaum 2006; Robin et al. 2001), little is known about the mtCYP2E1 metabolism of substrates, its relative significance compared to erCYP2E1, the mechanisms altering their contributions, and corresponding effects the biological consequences of CYP2E1 activity. Further research is clearly needed to address these knowledge gaps and our findings provide critical biochemical mechanisms for integrating CYP2E1 activity within biological processes to better understand the link between CYP2E1 metabolism and potential toxicological outcomes.

Acknowledgments

The authors gratefully acknowledge the assistance of Swapnali Halder for helping prepare rat tissues for the study, as well as Anthony Rusher for his assistance purifying subcellular fractions for catalytic assays. Financial support was provided in part by the Arkansas INBRE program, with grants from the National Center for Research Resources – NCRR (P20RR016460), the National Institute of General Medical Sciences – NIGMS (P20 GM103429) from the National Institutes of Health. The National Science Foundation Graduate Research Fellowship provided further funding support through a Graduate Research Fellowship Award to JHH (DGE 1452779).

References

1. Rep Carcinog Backgr Doc. National Toxicology Program; 2008. Final Report on Carcinogens Background Document for Styrene; p. i-398.
2. Addya S, Anandatheerthavarada HK, Biswas G, Bhagwat SV, Mullick J, Avadhani NG. Targeting of NH_2-terminal-processed microsomal protein to mitochondria: a novel pathway for the biogensis of hepatic mitochondrial P450MT2. J Cell Biol. 1997; 139:589–599. [PubMed: 9348277]
3. Amato G, Longo V, Mazzaccaro A, Gervasi PG. Chlorzoxazone 6-hydroxylase and *P*-nitrophenol hydroxylase as the most suitable activities for assaying cytochrome P450 2E1 in cynomolgus monkey liver. Drug Metab Dispos. 1998; 26:483–489. [PubMed: 9571230]

4. Anandatheerthavarada HK, Addya S, Dwivedi RS, Biswas G, Mullick J, Avadhani NG. Localization of multiple forms of inducible cytochromes P450 in rat liver mitochondria: immunological characteristics and patterns of xenobiotic substrate metabolism. Arch Biochem Biophys. 1997; 339:136–150. [PubMed: 9056243]
5. A.f.T.S.a.D. Registery. , editor. ATSDR. Detailed Data Table For The 2011 Priority List Of Hazardous Substances. U.S. Department of Health and Human Services, Public Health Service; 2011.
6. Bai J, Cederbaum AI. Overexpression of CYP2E1 in Mitochondria Sensitizes HepG2 Cells to the Toxicity Caused by Depletion of Glutathione. J Biol Chem. 2006; 281:5128–5136. [PubMed: 16380384]
7. Bansal S, Anandatheerthavarada HK, Prabu GK, Milne GL, Martin MV, Guengerich FP, Avadhani NG. Human Cytochrome P450 2E1 Mutations That Alter Mitochondrial Targeting Efficiency and Susceptibility to Ethanol-induced Toxicity in Cellular Models. J Biol Chem. 2013; 288:12627–12644. [PubMed: 23471973]
8. Barale R. The genetic toxicology of styrene and styrene oxide. Mutat Res. 1991; 257:107–126. [PubMed: 2005936]
9. Bonanni RC, Gatto MP, Paci E, Gordiani A, Gherardi M, Tranfo G. Biomonitoring for Exposure Assessment to Styrene in the Fibreglass Reinforced Plastic Industry: Determinants and Interferents. Ann Occup Hyg. 201510.1093/annhyg/mev047
10. Bond JA, Bolt HM. Review of The Toxicology of Styrene. Crit Rev Toxicol. 1989; 19:227–249. [PubMed: 2653733]
11. Charette SJ, Lambert H, Nadeau PJ, Landry J. Protein quantification by chemiluminescent Western blotting: Elimination of the antibody factor by dilution series and calibration curve. J Immunol Meth. 2010; 353:148–150.
12. Cohen MMJ, Leboucher GP, Livnat-Levanon N, Glickman MH, Weissman AM. Ubiquitin–Proteasome-dependent Degradation of a Mitofusin, a Critical Regulator of Mitochondrial Fusion. Mol Biol Cell. 2008; 19:2457–2464. [PubMed: 18353967]
13. Collom SL, Laddusaw RM, Burch AM, Kuzmic P, Perry MD Jr, Miller GP. CYP2E1 substrate inhibition: Mechanistic interpretation through an effector site for monocyclic compounds. J Biol Chem. 2008; 283:3487–3496. [PubMed: 18056994]
14. Evans MV, Caldwell JC. Evaluation of two different metabolic hypotheses for dichloromethane toxicity using physiologically based pharmacokinetic modeling for in vivo inhalation gas uptake data exposure in female B6C3F1 mice. Toxicol Appl Pharmacol. 2010; 244:280–290. [PubMed: 20153349]
15. Gregg C, Kyryakov P, Titorenko VI. Purification of Mitochondria from Yeast Cells. J Vis Exp. 2009:e1417.
16. Guengerich F. Rate-limiting steps in cytochrome P450 catalysis. Biol Chem. 2002; 383:1553–1564. [PubMed: 12452431]
17. Guengerich FP, Martin MV, Sohl CD, Cheng Q. Measurement of cytochrome P450 and NADPH-cytochrome P450 reductase. Nat Protocols. 2009; 4:1245–1251. [PubMed: 19661994]
18. Halpert JR, Guengerich FP, Bend JR, Correia MA. Selective inhibitors of cytochromes P450. Toxicol Appl Pharmacol. 1994; 125:163–175. [PubMed: 8171425]
19. Hargreaves MB, Jones BC, Smith DA, Gescher A. Inhibition of *p*-nitrophenol hydroxylase in rat liver microsomes by small aromatic and heterocyclic molecules. Drug Metab Dispos. 1994; 22:806–810. [PubMed: 7835233]
20. Harrelson JP, Atkins WM, Nelson SD. Multiple-Ligand Binding in CYP2A6: Probing Mechanisms of Cytochrome P450 Cooperativity by Assessing Substrate Dynamics. Biochemistry. 2008; 47:2978–2988. [PubMed: 18247580]
21. Hartman JH, Boysen G, Miller GP. CYP2E1 Metabolism of Styrene Involves Allostery. Drug Metab Dispos. 2012; 40:1976–1983. [PubMed: 22807108]
22. Hartman JH, Boysen G, Miller GP. Cooperative effects for CYP2E1 differ between styrene and its metabolites. Xenobiotica. 2013a; 43:755–764. [PubMed: 23327532]

23. Hartman JH, Bradley AM, Laddusaw RM, Perry MD Jr, Miller GP. Structure of pyrazole derivatives impact their affinity, stoichiometry, and cooperative interactions for CYP2E1 complexes. Arch Biochem Biophys. 2013b; 537:12–20. [PubMed: 23811196]
24. Hartman JH, Knott K, Miller GP. CYP2E1 hydroxylation of aniline involves negative cooperativity. Biochem Pharmacol. 2014a; 87:523–533. [PubMed: 24345333]
25. Hartman JH, Miller GP, Boysen G. Inhibitory potency of 4-carbon alkanes and alkenes toward CYP2E1 activity. Toxicol. 2014b; 318:51–58.
26. Kim H, Wang RS, Elovaara E, Raunio H, Pelkonen O, Aoyama T, Vainio H, Nakajima T. Cytochrome P450 isozymes responsible for the metabolism of toulene and stryene in human liver microsomes. Xenobiotica. 1997; 27:657–665. [PubMed: 9253143]
27. Knockaert L, Descatoire V, Vadrot N, Fromenty B, Robin MA. Mitochondrial CYP2E1 is sufficient to mediate oxidative stress and cytotoxicity induced by ethanol and acetaminophen. Toxicol in Vitro. 2011; 25:475–484. [PubMed: 21130154]
28. Koop DR. Hydroxylation of *p*-nitrophenol by rabbit ethanol-inducible cytochrome P-450 isozyme 3a. Mol Pharmacol. 1986; 29:399–404. [PubMed: 3702859]
29. Kuzmic P. Program DYNAFIT for the analysis of enzyme kinetic data: application to HIV protease. Anal Biochem. 1996; 237:260–273. [PubMed: 8660575]
30. Levy JW, Hartman JH, Perry MD Jr, Miller GP. Structural basis for cooperative binding of azoles to CYP2E1 as interpreted through guided molecular dynamics simulations. J Mol Graph Model. 2015; 56:43–52. [PubMed: 25544389]
31. Li D, Han Y, Meng X, Sun X, Yu Q, Li Y, Wan L, Huo Y, Guo C. Effect of Regular Organic Solvents on Cytochrome P450-Mediated Metabolic Activities in Rat Liver Microsomes. Drug Metab Dispos. 2010; 38:1922–1925. [PubMed: 20729275]
32. Löf A, Lundgren E, Nydahl EM, Nordqvist MB. Biological monitoring of styrene metabolites in blood. Scand J Work Environ Health. 1986; 12:70–74. [PubMed: 3961444]
33. Martignoni M, Groothuis GM, de Kanter R. Species differences between mouse, rat, dog, monkey and human CYP-mediated drug metabolism, inhibition and induction. Expert Opin Drug Metab Toxicol. 2006; 2:875–894. [PubMed: 17125407]
34. Mendrala A, Langvardt PW, Nitschke KD, Quast JF, Nolan RJ. In vitro kinetics of styrene and styrene oxide metabolism in rat, mouse, and human. Arch Toxicol. 1993; 67:18–27. [PubMed: 8452475]
35. Miller GP. Advances in the Interpretation and Prediction of CYP2E1 Metabolism from a Biochemical Perspective. Expert Opin Drug Metab Toxicol. 2008; 4:1053–1064. [PubMed: 18680440]
36. Nakajima T, Elovaara E, Gonzalez FJ, Gelboin HV, Raunio H, Pelkonen O, Vainio H, Aoyama T. Styrene metabolism by cDNA-expressed human hepatic and pulmonary cytochromes P450. Chem Res Toxicol. 1994; 7:891–896. [PubMed: 7696548]
37. Neve EPA, Ingelman-Sundberg M. A soluble NH_2-terminally truncated catalytically active form of rat cytochrome P450 2E1 targeted to liver mitochondria. FEBS Lett. 1999; 460:309–314. [PubMed: 10544255]
38. Newton DJ, Wang RW, Lu AY. Cytochrome P450 inhibitors. Evaluation of specificities in the in vitrometabolism of therapeutic agents by human liver microsomes. Drug Metab Dispos. 1995; 23:154–158. [PubMed: 7720520]
39. Pianalto KM, Hartman JH, Boysen G, Miller GP. Differences in butadiene adduct formation between rats and mice not due to selective inhibition of CYP2E1 by butadiene metabolites. Toxicol Lett. 2013; 223:221–227. [PubMed: 24021170]
40. Prieto M, Marhuenda D, Cardona A. Analysis of styrene and its metabolites in blood and urine of workers exposed to both styrene and acetone. J Anal Toxicol. 2002; 26:23–28. [PubMed: 11888014]
41. Raza H, Prabu SK, Robin MA, Avadhani NG. Elevated Mitochondrial Cytochrome P450 2E1 and Glutathione S-Transferase A4-4 in Streptozotocin-Induced Diabetic Rats: Tissue-Specific Variations and Roles in Oxidative Stress. Diabetes. 2004; 53:185–194. [PubMed: 14693714]
42. Real AM, Hong S, Pissios P. Nicotinamide N-Oxidation by CYP2E1 in Human Liver Microsomes. Drug Metab Dispos. 2013; 41:550–553. [PubMed: 23418369]

43. Robin MA, Anandatheerthavarada HK, Biswas G, Sepuri NBV, Gordon DM, Pain D, Avadhani NG. Bimodal Targeting of Microsomal CYP2E1 to Mitochondria through Activation of an N-terminal Chimeric Signal by cAMP-mediated Phosphorylation. J Biol Chem. 2002; 277:40583–40593. [PubMed: 12191992]
44. Robin MA, Anandatheerthavarada HK, Fang JK, Cudic M, Otvos L, Avadhani NG. Mitochondrial Targeted Cytochrome P450 2E1 (P450 MT5) Contains an Intact N Terminus and Requires Mitochondrial Specific Electron Transfer Proteins for Activity. J Biol Chem. 2001; 276:24680–24689. [PubMed: 11325963]
45. Robin MA, Sauvage I, Grandperret T, Descatoire V, Pessayre D, Fromenty B. Ethanol increases mitochondrial cytochrome P450 2E1 in mouse liver and rat hepatocytes. FEBS Lett. 2005; 579:6895–6902. [PubMed: 16337197]
46. Sangar MC, Bansal S, Avadhani NG. Bimodal targeting of microsomal cytochrome P450s to mitochondria: implications in drug metabolism and toxicity. Exp Opin Drug Metab Toxicol. 2010; 6:1231–1251.
47. Sittig, M. Handbook of Toxic And Hazardous Chemicals. Noyes Data Corporation; Park Ridge, NJ: 1981. p. 31
48. Smith PK, Krohn RI, Hermanson GT, Mallia AK, Gartner FH, Provenzano MD, Fujimoto EK, Goeke NM, Olson BJ, Klenk DC. Measurement of protein using bicinchoninic acid. Anal Biochem. 1985; 150:76–85. [PubMed: 3843705]
49. Somorovska M, Jahnova E, Tulinska J, Zamecnikova M, Sarmanova J, Terenova A, Vodickova L, Liskova A, Vallova B, Soucek P, Hemminki K, Norppa H, Hirvonen A, Tates AD, Fuortes L, Dusinska M, Vodicka P. Biomonitoring of occupational exposure to styrene in a plastics lamination plant. Mutat Res. 1999; 428:255–269. [PubMed: 10517998]
50. Taavitsainen P, Juvonen R, Pelkonen O. In Vitro Inhibition of Cytochrome P450 Enzymes in Human Liver Microsomes by a Potent CYP2A6 inhibitor, trans-2- Phenylcyclopropylamine (Tranylcypromine), and Its Nonamine Analog, Cyclopropylbenzene. Drug Metab Dispos. 2001; 29:217–222. [PubMed: 11181487]
51. Tassaneeyakul W, Veronese ME, Birkett DJ, Gonzalez FJ, Miners JO. Validation of 4-nitrophenol as an *in vitro* substrate probe for human liver CYP2E1 using cDNA expression and microsomal kinetic techniques. Biochem Pharmacol. 1993; 46:1975–1981. [PubMed: 8267647]
52. Velick SF, Strittmatter P. The oxidation-reduction stoichiometry and potential of microsomal cytochrome b_5. J Biol Chem. 1956; 221:265–275. [PubMed: 13345816]
53. Zerilli A, Ratanasavanh D, Lucas D, Goasduff T, Dreano Y, Menard C, Picart D, Berthou F. Both cytochromes P450 2E1 and 3A are involved in the O-hydroxylation of *p*-Nitrophenol, a catalytic activity known to be specific for P450 2E1. Chem Res Toxicol. 1997; 10:1205–1212. [PubMed: 9348445]
54. Zhang D, Wang L, Chandrasena G, Ma L, Zhu M, Zhang H, Davis CD, Humphreys WG. Involvement of Multiple Cytochrome P450 and UDP-Glucuronosyltransferase Enzymes in the in Vitro Metabolism of Muraglitazar. Drug Metab Dispos. 2007; 35:139–149. [PubMed: 17062778]
55. Zhang W, Kilicarslan T, Tyndale RF, Sellers EM. Evaluation of Methoxsalen, Tranylcypromine, and Tryptamine as Specific and Selective CYP2A6 Inhibitors in Vitro. Drug Metab Dispos. 2001; 29:897–902. [PubMed: 11353760]
56. Zheng N, Zou P, Wang S, Sun D. In Vitro Metabolism of 17-(Dimethylaminoethylamino)-17-demethoxygeldanamycin in Human Liver Microsomes. Drug Metab Dispos. 2011; 39:627–635. [PubMed: 21177985]

Abbreviations

CYP	cytochrome P450 (specific isoforms)
SDHA	succinate dehydrogenase
SERCA	Sarco/endoplasmic reticulum Ca^{2+}-ATPase

Highlights

- Metabolically active CYP2E1 localizes to the endoplasmic reticulum and mitochondria.
- CYP2E1 localization impacts substrate affinity, stoichiometry, and turnover.
- Toxicological relevance of CYP2E1 subcellular localization may depend on substrate.

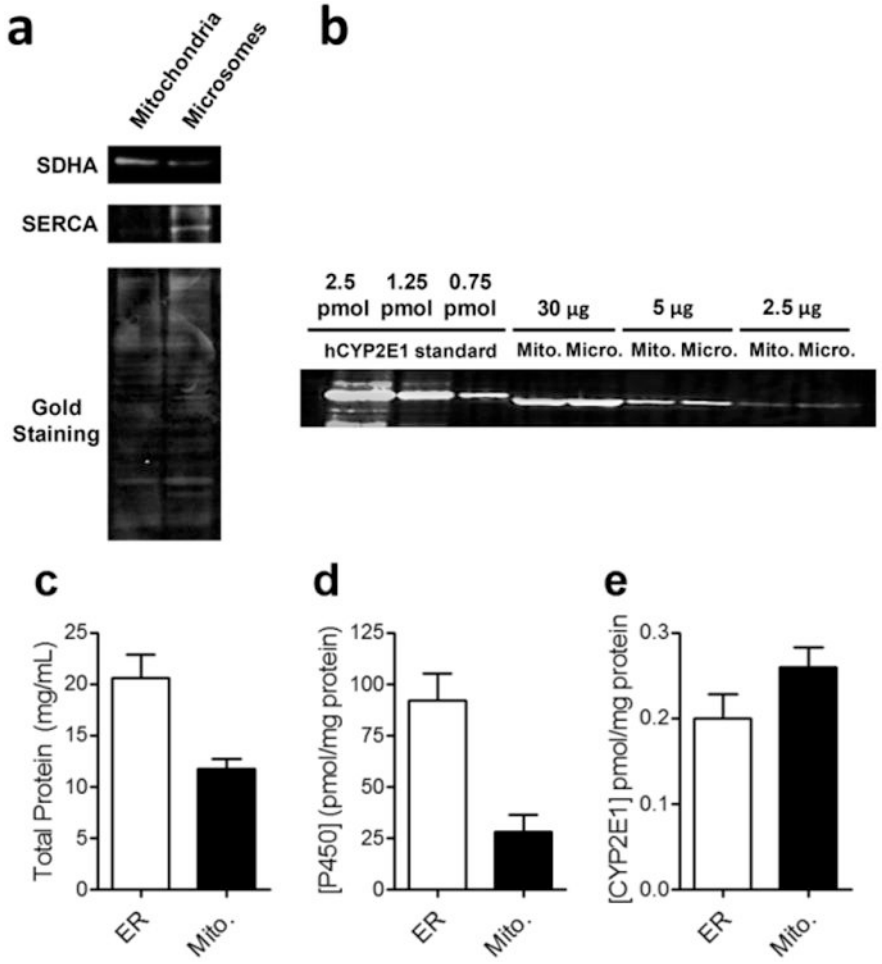

Figure 1.

Characterization of purified rat hepatic subcellular fractions: representative immunoblots for fraction purity (Panel A) and CYP2E1 content (Panel B), quantification of total protein per volume of purified fractions (Panel C), total P450 per milligram protein (Panel D), and total CYP2E1 per milligram protein (Panel E). Proteins in each fraction were resolved by gel electrophoresis on SDS-polyacrylamide, transferred to nitrocellulose membranes, and immunoblotted using specific antibodies. For testing fraction purity, succinate dehydrogenase (SDHA) was used as a marker of mitochondria and sarco/endoplasmic reticulum Ca^{2+}-ATPase (SERCA) was used as a marker for microsomes. For quantifying CYP2E1, human recombinant CYP2E1 Supersomes® (Corning Gentest) were obtained commercially and used as an authentic standard. CYP2E1 bands were quantified from the standards and fractions using densitometry and CYP2E1 concentration was calculated based on the standard curve. Protein content was assayed using the Pierce bicinchoninic acid (BCA) assay; P450 content was determined using reduced CO spectra as described (Guengerich et al. 2009); CYP2E1 content was determined using immunoblot with densitometry to quantify levels by comparison to a standard curve obtained with human CYP2E1 Supersomes® (Corning Gentest).

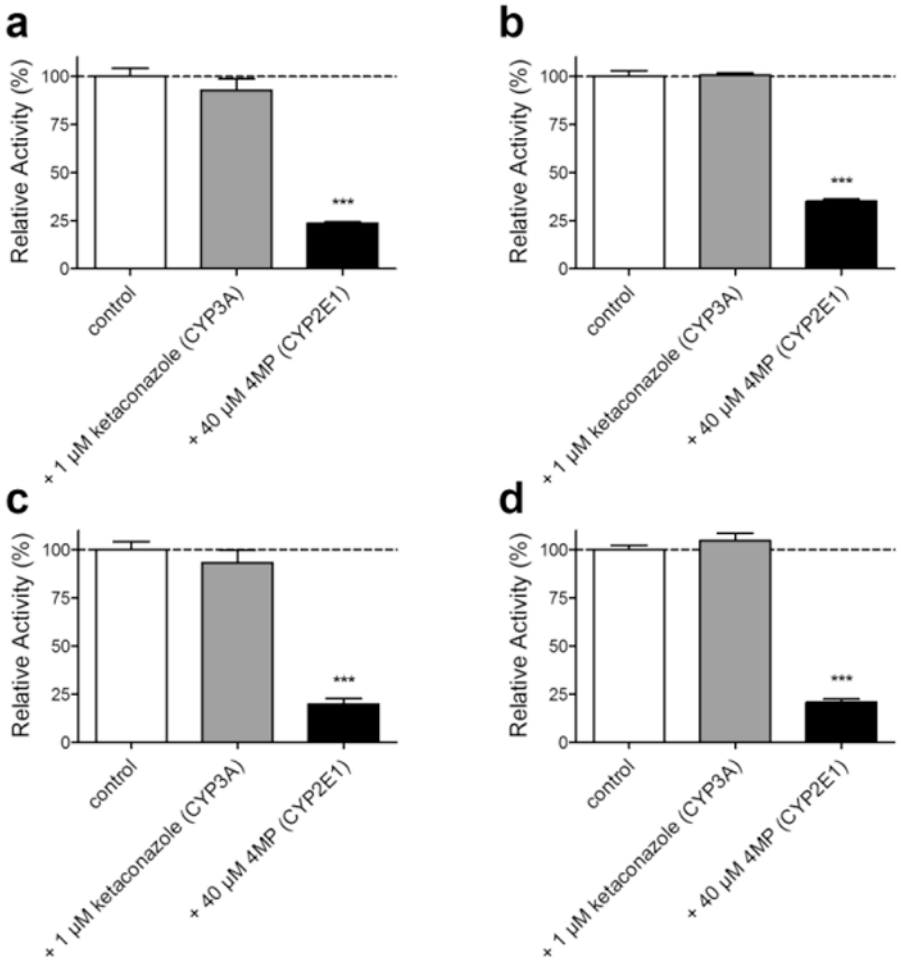

Figure 2.

Inhibitor phenotyping of steady-state oxidation of 4-nitrophenol by rat liver microsomes (Panels A and B) and mitochondria (Panels C and D). For reactions, 0.5 mg/mL rat liver microsomes or 2 mg/mL rat liver mitochondrial fractions, 4-nitrophenol (50 μM for panels A and C, 500 μM for Panels B and D), and 1 mM NADPH were incubated at 37°C and pH 7.4 in the absence (white bars) or presence (grey bars) of specific inhibitors for each P450 isoform reported to metabolize 4-nitrophenol. Activity was normalized to control (100%) and reported as percent activity. Control (uninhibited, containing methanol only) rates of mtCYP2E1 4-nitrophenol oxidation were 26 and 60 pmol/min/pmol CYP2E1 for 50 and 500 μM 4-nitrophenol, respectively. Control rates for erCYP2E1 were 290 and 1080 pmol/min/pmol CYP2E1 for 50 and 500 μM 4-nitrophenol, respectively. Reported activities represent the average of at least three individual experiments, including the mean ± standard deviation. Asterisks indicate statistical significance of inhibition compared to control (***, $p<0.001$). KCZ, ketoconazole; 4MP, 4-methylpyrazole.

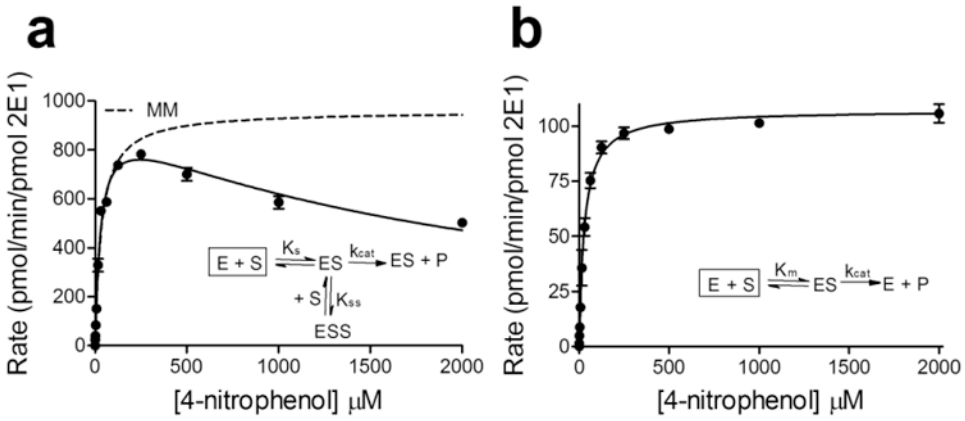

Figure 3.

Steady-state kinetics of hydroxylation of 4-nitrophenol by rat liver microsomes (Panel A) and mitochondrial fractions (Panel B). In each panel, the solid line represents the fit of the data to the statistically preferred mechanism based on Akaike Information Criterion using GraphPad Prism 5.0. In Panel A, the dashed line represents the fit of the data to the Michaelis-Menten equation for comparison. For reactions, 0.5 mg/mL rat liver microsomes or 2 mg/mL rat liver mitochondrial fractions, 4-nitrophenol (varied from 10 to 2000 μM), and 1 mM NADPH were incubated at 37°C and pH 7.4. Reported values represent the average of at least five experimental replicates.

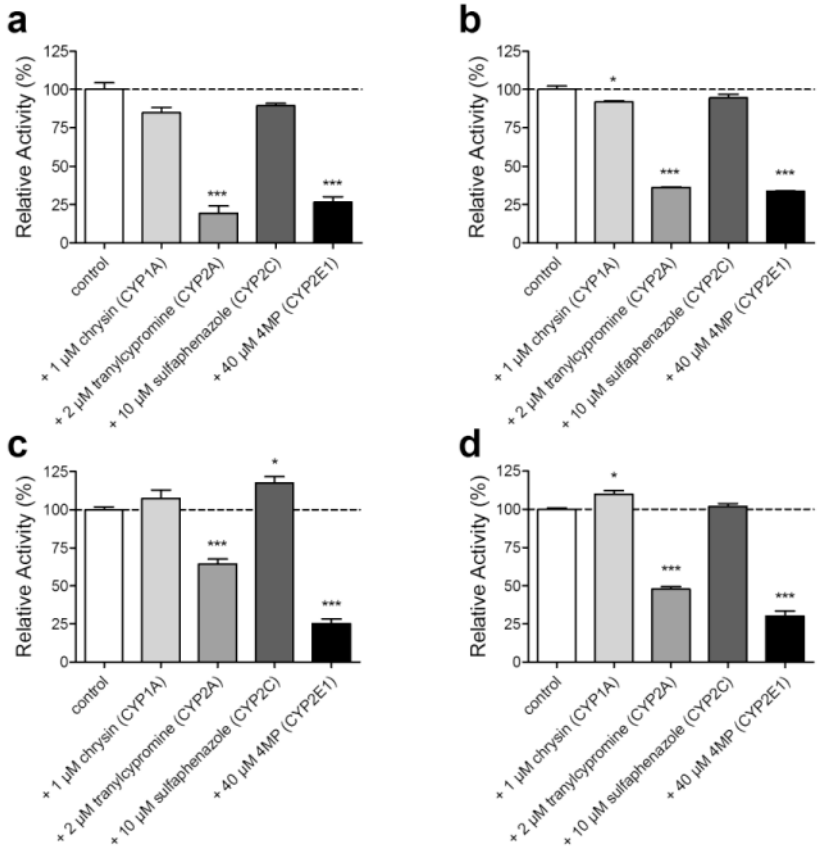

Figure 4.

Inhibitor phenotyping of steady-state oxidation of aniline by rat liver microsomes (Panels A and B) and mitochondrial fractions (Panels C and D). For reactions, 0.5 mg/mL rat liver microsomes or 2 mg/mL rat liver mitochondrial fractions, aniline (50 μM for Panels A and C, 500 μM for Panels B and D), and 1 mM NADPH were incubated at 37°C and pH 7.4 in the absence (white bars) or presence (grey bars) of specific inhibitors for each P450 isoform reported to be involved in 4-hydroxylation of aniline. Activity was normalized to control (100%) and reported as percent activity. Control (uninhibited, containing methanol only) rates of mtCYP2E1 aniline hydroxylation were 28 and 58 pmol/min/pmol CYP2E1 for 50 and 500 μM aniline, respectively. Control rates for erCYP2E1 were 260 and 1000 pmol/min/mg for 50 and 500 μM aniline, respectively. Reported activities represent the average of at least three individual experiments, including the mean ± standard deviation. Asterisks indicate statistical significance of inhibition compared to control (*, $p<0.05$; ***, $p<0.001$). Chrysin, CHS; tranylcypromine, TCP; sulfaphenazole, SPA; 4-methylpyrazole, 4MP.

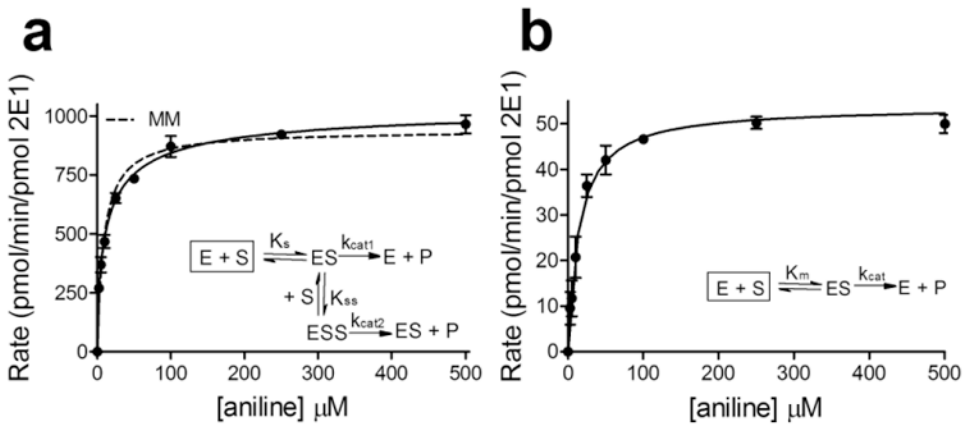

Figure 5.

Steady-state kinetics of aniline hydroxylation by rat liver microsomes (Panel A) and mitochondria (Panel B). In each panel, the solid line represents the fit of the data to the statistically preferred mechanism based on Akaike Information Criterion using GraphPad Prism 5.0. In Panel A, the dashed line represents the fit of the data to the Michaelis-Menten equation for comparison. For reactions, 0.5 mg/mL rat liver microsomes or 2 mg/mL rat liver mitochondrial fractions, aniline (varied from 2.5 to 500 μM), and 1 mM NADPH were incubated at 37°C and pH 7.4. Reported values represent the average of at least four experimental replicates.

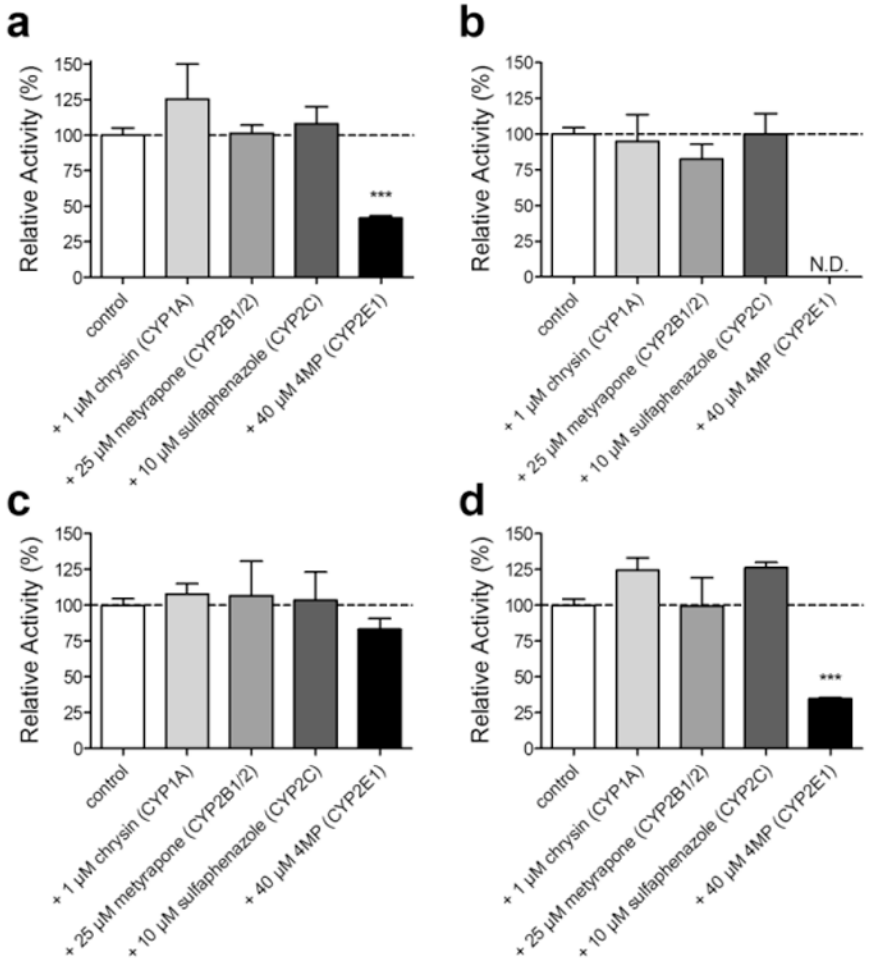

Figure 6.

Inhibitor phenotyping of steady-state oxidation of styrene by rat liver microsomes (Panels A and B) and mitochondrial fractions (Panels C and D). For reactions, 0.5 mg/mL rat liver microsomes or 2 mg/mL rat liver mitochondrial fractions, styrene (50 μM for Panels A and C, 500 μM for Panels B and D), and 1 mM NADPH were incubated at 37°C and pH 7.4 in the absence (white bars) or presence (grey bars) of specific inhibitors for each P450 isoform reported to be involved in epoxidation of styrene. Activity was normalized to control (100%) and reported as percent activity. Control (uninhibited, containing methanol only) rates of mtCYP2E1 styrene oxidation were 54 and 76 pmol/min/pmol CYP2E1 for 50 and 500 μM styrene, respectively. Control rates for erCYP2E1 were 310 and 390 pmol/min/mg for 50 and 500 μM styrene, respectively. Reported activities represent the average of at least three individual experiments, including the mean ± standard deviation. Asterisks indicate statistical significance of inhibition compared to control (***, $p<0.001$). Chrysin, CHS; metyrapone, MTP; sulfaphenazole, SPA; 4-methylpyrazole, 4MP.

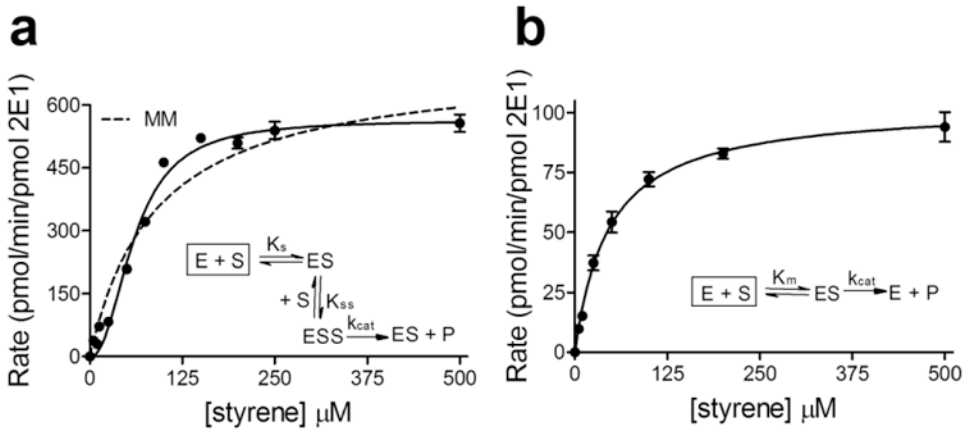

Figure 7.

Steady-state kinetics of styrene oxidation by rat liver microsomes (Panel A) and mitochondrial fractions (Panel B). In each panel, the solid line represents the fit of the data to the statistically preferred mechanism based on Akaike Information Criterion using GraphPad Prism 5.0. In Panel A, the dashed line represents the fit of the data to the Michaelis-Menten equation for comparison. For reactions, 0.5 mg/mL rat liver microsomes or 2 mg/mL rat liver mitochondrial fractions, styrene (varied from 5 to 500 μM), and 1 mM NADPH were incubated at 37°C and pH 7.4. Reported values represent the average of at least three experimental replicates.

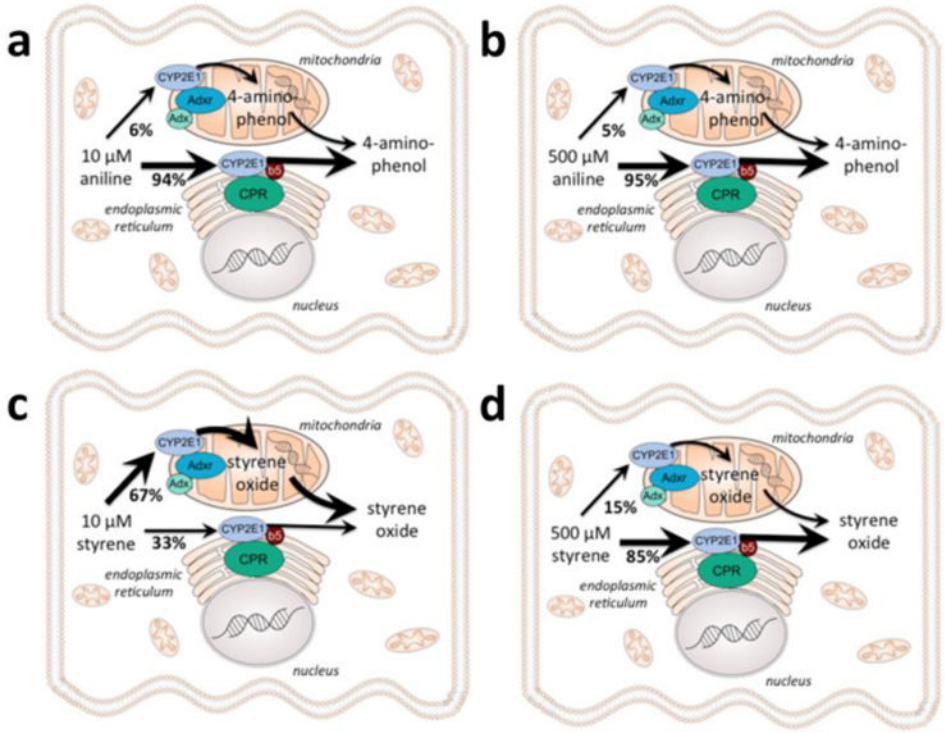

Figure 8.

Stylized depiction of the theoretical metabolic flux by mitochondrial and microsomal CYP2E1 at low and high pollutant concentrations. Aniline shown in Panels A and B, while styrene depicted in Panels C and D. For estimation of metabolic flux, rates were calculated from the fit of the steady-state kinetic data to the preferred mechanism and summed to represent total metabolism (100%) at that concentration. Then the relative contribution from each compartment was expressed as a percent of total metabolism.

Table 1

Compound	Enzyme Source	Preferred Mechanism	K_m or K_s [a]	K_{ss} [a]	k_{cat} [b]	k_{cat2} [b]
4-nitrophenol	microsomes	Two-Site Model, ES active only	28 (24 to 34)	2000 (1600 to 2600)	940 (880 to 1000)	-
	mitochondria	One-Site Model (Michaelis-Menten)	28 (24 to 33)	-	110 (100 to 110)	-
aniline	microsomes	Two-Site Model, ES and ESS active	2.1 (0.010 to 5.2)	54 (21 to 550)	500 (230 to 770)	1000 (970 to 1300)
	mitochondria	One-Site Model (Michaelis-Menten)	10 (7.5 to 12)	-	52 (49 to 54)	-
styrene	microsomes	Two-Site Model, ESS active only	100 (31 to 2600)	32 (2 to 64)	630 (580 to 690)	-
	mitochondria	One-Site Model (Michaelis-Menten)	45 (36 to 56)	-	100 (96 to 110)	-

[a] Kinetic constants K_m, K_s, and K_{ss} are expressed in μM

[b] Rates k_{cat} and k_{cat2} are expressed in pmol/min/pmol CYP2E1